

Fidelity spectrum and phase transitions of quantum systems

P. D. Sacramento¹, N. Paunković², V. R. Vieira¹

¹ *Departamento de Física and CFIF, Instituto Superior Técnico,
TU Lisbon, Av. Rovisco Pais, 1049-001 Lisboa, Portugal and*

² *SQIG- Instituto de Telecomunicações, IST, TU Lisbon, Av. Rovisco Pais, 1049-001 Lisboa, Portugal*

Quantum fidelity between two density matrices, $F(\rho_1, \rho_2)$ is usually defined as the trace of the operator $\mathcal{F} = \sqrt{\sqrt{\rho_1}\rho_2\sqrt{\rho_1}}$. We study the logarithmic spectrum of this operator, which we denote by *fidelity spectrum*, in the cases of the XX spin chain in a magnetic field, a magnetic impurity inserted in a conventional superconductor and a bulk superconductor at finite temperature. When the density matrices are equal, $\rho_1 = \rho_2$, the fidelity spectrum reduces to the entanglement spectrum. We find that the fidelity spectrum can be a useful tool in giving a detailed characterization of different phases of many-body quantum systems.

I. INTRODUCTION

A quantum system in a pure state is described by a density matrix which is just a projector onto that state. At zero temperature it is the projector to the groundstate of the system. In general, the Hamiltonian of the system is a function of some parameters which determine the groundstate. The quantum fidelity between two states (for two sets of parameters) is, in this simple case, the absolute value of the overlap between the groundstates for the two sets of parameters. When the system is in a mixed state the density matrix is more complex. Typical situations that lead to mixed states are: i) reduced density matrices where a trace over some degrees of freedom is carried out, or ii) systems at finite temperatures where the density matrix may be taken as the Boltzmann factor over the energy eigenstates.

In general the quantum fidelity [1] between two states characterized by two density matrices ρ_1 and ρ_2 may be defined as the trace of the fidelity operator, \mathcal{F} ,

$$F(\rho_1, \rho_2) = \text{Tr}\mathcal{F} = \text{Tr}\sqrt{\sqrt{\rho_1}\rho_2\sqrt{\rho_1}}. \quad (1)$$

One may also consider the spectrum of the fidelity operator $\mathcal{F}(\rho_1, \rho_2)$. Its set of eigenvalues λ_i , which we denote *fidelity operator spectrum*, and $-\ln \lambda_i$, which we call the *fidelity spectrum*, may provide more information as compared to the fidelity (its trace), in a way parallel to the extra information provided by the entanglement spectrum [2], as compared to the von Neumann entropy.

In the case of pure states $\rho_1 = |GS_1\rangle\langle GS_1|$ and $\rho_2 = |GS_2\rangle\langle GS_2|$ the fidelity is just the norm of the overlap

$$F(\rho_1, \rho_2) = |\langle GS_1|GS_2\rangle|. \quad (2)$$

If the two states are the same it is just the normalization of the state (taken as 1). In the case of two equal mixed states the fidelity is just

$$F(\rho, \rho) = \text{Tr}\rho = 1 \quad (3)$$

and the operator \mathcal{F} in this case has a set of eigenvalues, $\lambda_i = \lambda_i^\rho$, such that $-\ln \lambda_i$ is called the entanglement spectrum, and has received considerable attention lately [2].

In this work we will analyse the fidelity spectrum for several physical systems paying particular attention to the vicinity of quantum phase transitions (QPT) as well as the properties characterizing their quantum phases.

The interplay between quantum information and condensed matter physics has been extensively considered using entanglement as a measure for the behavior of many body systems [3]. The distinguishability between states has been used as a possible criterion to study quantum phase transitions [4]. By its own nature, fidelity between pure groundstates signals a change of state as one approaches a quantum phase transition [5]. The fidelity between mixed states has also been used as a signature of quantum phase transitions [6, 7] and to distinguish between different states of matter at finite temperatures [8]. A standard measure of entanglement in a system is the von Neumann entropy. However, as argued in Ref. [2], more information about a mixed state is obtained if the entanglement spectrum is analysed. Considering reduced density matrices where part of the degrees of freedom are integrated over, such as dividing the system in real space into two parts A and B , it was shown in the context of the quantum Hall effect [2, 9] and in the context of coupled spin chains [10], that the groundstate entanglement spectrum of A contains information about excited energy states of the frontier of the subsystem A . In particular, in the quantum Hall effect the entanglement spectrum of the bulk system has a low-lying structure of levels that matches the edge states, and in the case of two coupled Heisenberg spin chains, considering the subsystem A as one of the chains, the entanglement

spectrum has a structure that matches the energy excitations of a single Heisenberg chain. Other partitionings of the system have been proposed that lead to further information [11] and considering a partitioning in momentum space it was shown that information about energy excitations of a single Heisenberg chain is contained in the groundstate wave function through the entanglement spectrum [12].

In this work we consider the fidelity spectrum of various systems. While the entanglement spectrum has some relation to the energy spectrum of the edge states or even bulk states, the fidelity spectrum contains information about which eigenvalues have a larger contribution to the distinguishability between quantum states. We start by considering two systems at zero temperature: a magnetic impurity inserted in a conventional superconductor and the XX chain in a magnetic field. In the first case, described in Section II, the magnetic impurity is coupled through a spin interaction to the spin density of the conduction electrons, tuned by a coupling J . As previously discussed [7, 13, 14], as the coupling J grows, the system goes through a first order phase transition. At this point the system becomes magnetized and various quantities such as local density of states, spin content, gap function and quantum information measures can be used to detect this transition. For instance, various entanglement measures [15] and the partial state fidelity itself [7] have been used before. In the case of the XX chain describing spins $1/2$ confined to a plane (xy) and with a transverse magnetic field h , aligned along the z direction (Section III), there is a quantum phase transition from a XX phase, where the spins are aligned in the xy plane, if the magnetic field is small, and an Ising-like phase where the spins point along the field direction, if the field is strong enough. Considering the coupling between the spins as the energy scale, the second order transition occurs at the point $h_c = 1$. This transition is also signaled in various ways such as the decrease of the fidelity near the critical point [4]. In Section IV we consider thermal states in a conventional superconductor.

II. MAGNETIC IMPURITY IN A SUPERCONDUCTOR

Consider first a classical spin immersed in a two-dimensional s -wave conventional superconductor. We use a lattice description of the system. In the center of the system, $i = l_c = (0, 0)$, we place a classical spin along the z -direction $\vec{S} = S\vec{e}_z$, with no loss of generality. The Hamiltonian of the system is given by

$$H = - \sum_{\langle ij \rangle \sigma} t_{ij} c_{i\sigma}^\dagger c_{j\sigma} - \varepsilon_F \sum_{i\sigma} c_{i\sigma}^\dagger c_{i\sigma} + \sum_i \left(\Delta_i c_{i\uparrow}^\dagger c_{i\downarrow}^\dagger + \Delta_i^* c_{i\downarrow} c_{i\uparrow} \right) - \sum_{\sigma\sigma'} J c_{l_c\sigma}^\dagger \sigma_{\sigma\sigma'}^z c_{l_c\sigma'}, \quad (4)$$

where the first term describes the hopping of electrons between different sites on the lattice, ε_F is the chemical potential, the third term is the superconducting s -pairing with the site-dependent order parameter Δ_i , and the last term, with $J > 0$, is the exchange interaction between an electron at site $i = l_c$ and the magnetic impurity. The hopping matrix is given by $t_{ij} = t\delta_{j,i+\delta}$ where δ is a vector to a nearest-neighbor site. Note that both indices $i, j \in \{1, 2, \dots, N\}$ specify sites on a two-dimensional system (N is the number of sites). We take energy units in terms of t ($t = 1$), and choose $\varepsilon_F = -1$.

If we divide the whole system in two subsystems, say A and B , then the partial mixed state, given by the reduced density operator ρ_A for the subsystem A , is defined as

$$\rho_A = \text{Tr}_B \rho, \quad (5)$$

where $\text{Tr}_B[\cdot]$ represents the partial trace evaluated over the Hilbert space \mathcal{H}_B of the subsystem B . We take A to be one site, either the impurity site or an arbitrary site in the bulk far from the impurity such that ρ_1 and ρ_2 of Eq. (1) are one-site density matrices.

In many-body systems second quantization is the natural way to perform any calculation. The matrix elements of the density matrix are simply defined in terms of correlation functions of the whole system. For instance, in the case of the single-site partial mixed states using local basis states $\mathcal{B} = \{|0\rangle, |\uparrow\downarrow\rangle, |\uparrow\rangle, |\downarrow\rangle\}$, which denote the four possible states — unoccupied, double occupied, single occupied with an electron with spin up and single occupied with an electron with spin down, respectively — it can be shown that the corresponding density matrix reads as [7]

$$\rho_i = \begin{pmatrix} \langle (1 - n_\uparrow)(1 - n_\downarrow) \rangle & \langle c_\uparrow^\dagger c_\uparrow^\dagger \rangle & 0 & 0 \\ \langle c_\downarrow c_\uparrow \rangle & \langle n_\uparrow n_\downarrow \rangle & 0 & 0 \\ 0 & 0 & \langle n_\uparrow(1 - n_\downarrow) \rangle & \langle c_\downarrow^\dagger c_\uparrow \rangle \\ 0 & 0 & \langle c_\uparrow^\dagger c_\downarrow \rangle & \langle (1 - n_\uparrow)n_\downarrow \rangle \end{pmatrix}_i, \quad (6)$$

where the index i denotes the site. The spin and the charge parts decouple. The spin part couples the two spin orientations (single occupied states) and the charge part couples the empty and doubly occupied states. The diagonal

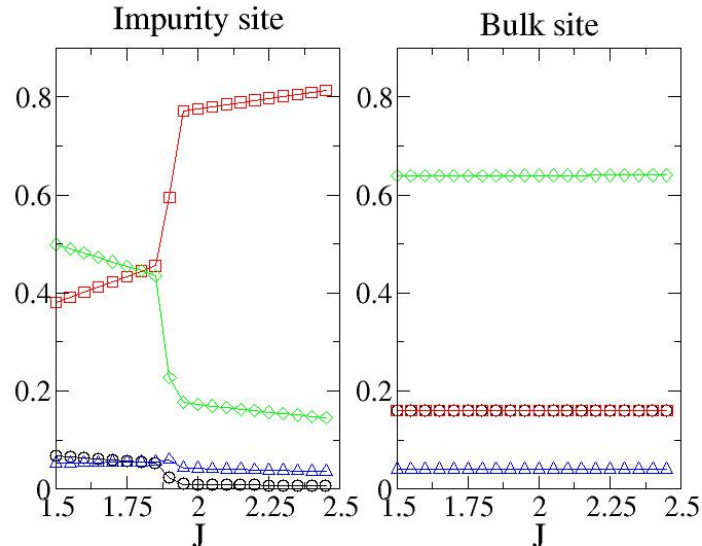


Figure 1: (color online) Fidelity operator spectrum at the impurity site (left) and at a bulk site (right) as a function of the spin coupling, J , where one density matrix is calculated at J and the other at $J + \delta J$, where $\delta J = 0.05$. In black and red is the charge contribution and in green and blue the spin contribution.

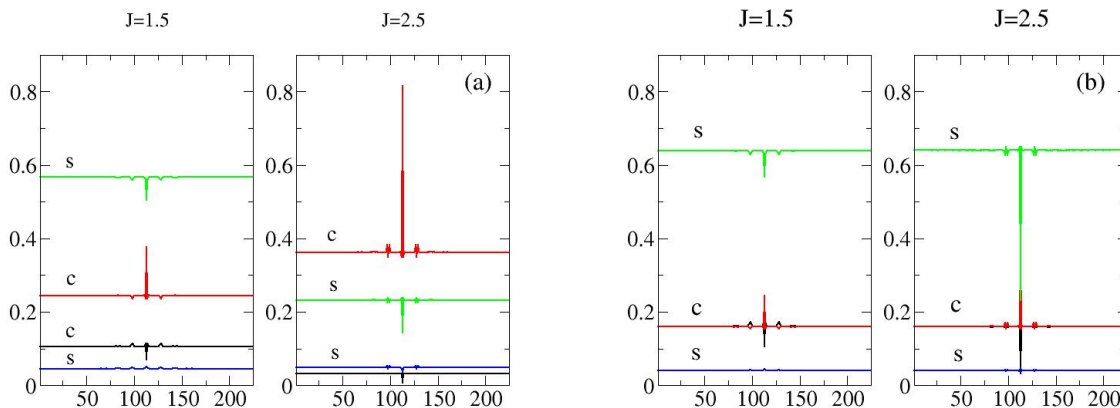


Figure 2: (color online) Fidelity operator spectrum: charge eigenvalues in black and red; spin eigenvalues in green and blue. System size is 15×15 . a) One of the sites is at the impurity, $i_1 = l_c$, and the other site, i_2 , is arbitrary. In the left panel $J_1 = J_2 = 1.5$, and in the right panel $J_1 = J_2 = 2.5$. b) One of the sites, i_1 , is a site in the bulk and the other site, i_2 , is arbitrary. The other parameters are the same as in a). Recall that $J = 1.5 < J_c$ and $J = 2.5 > J_c$.

terms of the matrix describe the number of empty sites, the number of doubly occupied sites, the number of spin up sites and the number of spin down sites, respectively. The sum of the diagonal terms is equal to 1 due to normalization. The matrix is easily diagonalized and the fidelity between two different one-site states obtained straightforwardly.

We will consider two density matrices of the form $\rho_1(J_1; i_1)$, and $\rho_2(J_2; i_2)$ for two values, J_1 and J_2 , of the spin coupling J , and for two sites, i_1 and i_2 .

In Fig. 1 we show the fidelity operator spectrum as a function of the coupling between the magnetic impurity and the electronic spin density taking $J_1 = J$, $J_2 = J + 0.05$ where $i_1 = i_2 = i$ is the impurity site or a bulk site. The charge and spin parts separate and in the charge part there is the empty and the doubly-occupied contributions and in the spin part the spin up and spin down contributions. As the coupling J grows there is a discontinuity in the eigenvalues. This discontinuity is associated with the quantum phase transition previously discussed. The sum of the

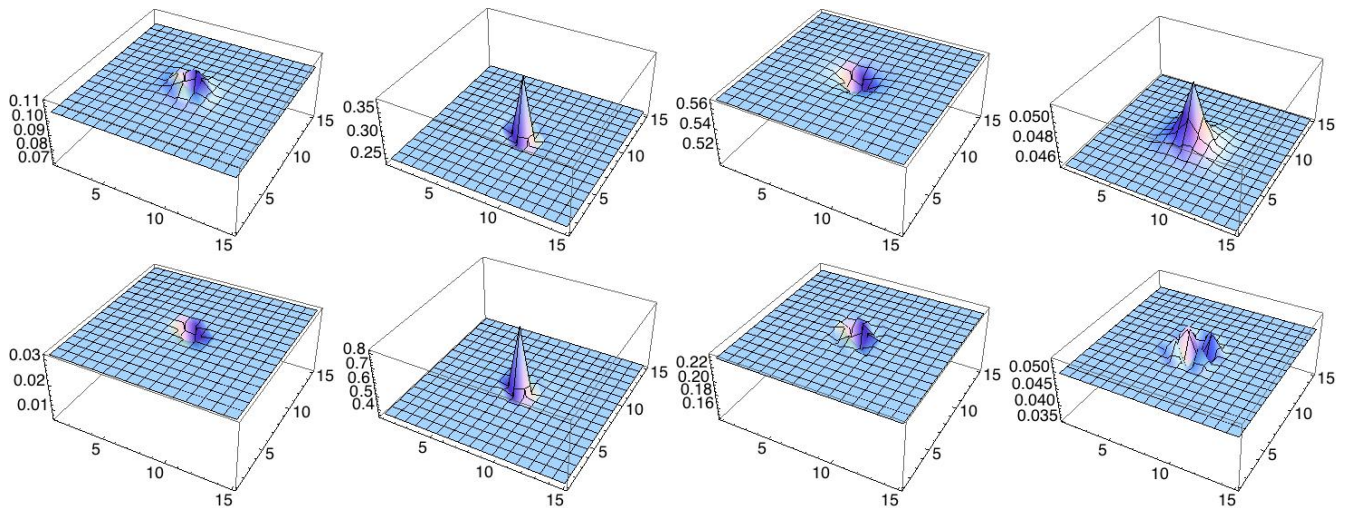


Figure 3: (color online) Fidelity operator spectrum as a function of space. System size is 15×15 . Top panels $J = 1.5$. Lower panels $J = 2.5$. From left to right, the first two panels are the charge eigenvalues and the right two panels the spin eigenvalues, for lattice sites $i_1 = l_c$ and i_2 an arbitrary site.

four eigenvalues is the fidelity, as discussed before. There is a discontinuity at the QPT both in the total fidelity, in the charge and spin parts and in the individual eigenvalues as well. As we can see, the discontinuities occur mainly in one of the charge eigenvalues and in one of the spin eigenvalues. As one crosses the QPT to a regime where the impurity captures one electron breaking a Cooper pair we see that the main contribution to the discontinuity in the charge part comes from the doubly-occupied states, where there is a significant increase at the QPT. In the same way there is a significant decrease in the spin up eigenvalue, leading to a smaller spin contribution beyond the QPT. For small values of J there is a screening of the perturbation induced by the magnetic impurity in the superconductor. A small fidelity means a higher degree of distinguishability. For small values of J the spin down eigenvalue is small but the spin up is still high. Beyond the QPT both contributions are small. This indicates that the transition is mainly of spin character: as the fidelity tends asymptotically to 1 away from the QPT and the spin eigenvalues are small, the charge eigenvalues have to compensate, however, mainly through the doubly-occupied contribution, as expected. Note that, in the bulk, the transition is quite small. The physics is very local, centered around the impurity site.

In Fig. 2 we consider that the coupling is fixed, but the two density matrices are calculated at different sites i_1 and i_2 : $\rho_1(J, i_1)$ and $\rho_2(J, i_2)$. The various cases are specified in the caption of the figure. In these figures the horizontal axis is the lattice site. For each site there are four eigenvalues. The central point is the impurity site. The symmetrical peaks close to the central point are the neighbors of the central point (please note that here we number the lattice sites of the 2d system as a 1d system sequentially row by row; so the lattice nearest neighbors in the x-direction are close by neighbors but the neighbors in the y direction are far apart). The fluctuations around the central peak are of course better seen in a 3d plot. This is shown in Fig. 3 where we compare the four eigenvalues with the results of Fig. 1a. As discussed above the empty site and the spin down contributions are small and do not change much as we change from $J = 1.5$ (below the QPT) to $J = 2.5$ (above the QPT).

III. XX SPIN-1/2 CHAIN IN A TRANSVERSE FIELD

The XX spin 1/2 model has been solved exactly via the Jordan-Wigner transformation where it is reduced to a system of free spinless fermions [16]. The correlation functions were also calculated [17] as well as the reduced density matrix of a system of L contiguous spins [18–20]. The information theoretic approach in terms fidelity, Fisher metric and Chernoff bound was applied to the XY model in [4, 21–26].

The Hamiltonian we will consider here is of the form

$$H = -\frac{1}{2} \sum_{l=0}^{N-1} \left(\frac{1+\gamma}{2} \sigma_l^x \sigma_{l+1}^x + \frac{1-\gamma}{2} \sigma_l^y \sigma_{l+1}^y + h \sigma_l^z \right). \quad (7)$$

Here the spin operators are described by Pauli matrices, h is the transverse magnetic field and γ is the anisotropy. We will simplify and consider $\gamma = 0$ and we take $0 < h < 1$. We will consider a block of L contiguous spins. The

reduced density matrix of the block can be written as [18]

$$\rho_A = \prod_{i=1}^L \left(\frac{1 + \nu_i}{2} b_i^\dagger b_i + \frac{1 - \nu_i}{2} b_i b_i^\dagger \right). \quad (8)$$

The operators b_i are spinless fermionic operators with a 2-state space (the eigenvalues of the number operator $n_i = b_i^\dagger b_i$ are 1 and 0, corresponding to occupied or empty state, respectively). The eigenvalues of the reduced density matrix are 2^L in number as the result of the direct product of the $i = 1, \dots, L$ subspaces. Defining two Majorana operators of the form

$$\begin{aligned} c_{2l-1} &= \left(\prod_{n=1}^{l-1} \sigma_n^z \right) \sigma_l^x \\ c_{2l} &= \left(\prod_{n=1}^{l-1} \sigma_n^z \right) \sigma_l^y \end{aligned} \quad (9)$$

in terms of the spin operators, it has been shown that

$$\langle GS | c_m c_n | GS \rangle = \delta_{m,n} + i (B_L)_{mn}. \quad (10)$$

The matrix B_L is written as

$$B_L = G_L \otimes \begin{pmatrix} 0 & 1 \\ -1 & 0 \end{pmatrix} \quad (11)$$

with

$$G_L = \begin{pmatrix} g_0 & g_{-1} & \cdot & \cdot & \cdot & g_{1-L} \\ g_1 & g_0 & \cdot & \cdot & \cdot & \cdot \\ \cdot & \cdot & \cdot & \cdot & \cdot & \cdot \\ \cdot & \cdot & \cdot & \cdot & \cdot & \cdot \\ \cdot & \cdot & \cdot & \cdot & \cdot & \cdot \\ g_{L-1} & \cdot & \cdot & \cdot & \cdot & g_0 \end{pmatrix}. \quad (12)$$

We have that $g_l = g_{-l}$, $g_0 = (2\varphi_c/\pi) - 1$ and $g_{l \neq 0} = (2/l\pi) \sin l\varphi_c$, where $\varphi_c = \arccos(h)$. Defining new Majorana fermions through the transformation $d = Vc$ and imposing that

$$\langle GS | d_m d_n | GS \rangle = \delta_{m,n} + i (\tilde{B}_L)_{mn} \quad (13)$$

with

$$\tilde{B}_L = V B_L V^T = \Omega \otimes \begin{pmatrix} 0 & 1 \\ -1 & 0 \end{pmatrix}, \quad (14)$$

where Ω is a diagonal matrix with L diagonal elements ν_l , leads to the diagonal form Eq. (8) of the reduced density matrix, ρ_A , having defined L complex fermionic fields like

$$b_l = \frac{d_{2l} + i d_{2l+1}}{2}. \quad (15)$$

The transformation V that block diagonalizes the problem depends on the Hamiltonian parameters through the numbers g_l .

In order to calculate the fidelity operator $\mathcal{F} = \sqrt{\sqrt{\rho_1} \rho_2 \sqrt{\rho_1}}$ one needs to consider the product of two reduced density matrices for two different magnetic fields. Even though each of the reduced density matrix can be diagonalized, the transformations needed to diagonalize ρ_1 and ρ_2 are different. The diagonalization of ρ_1 (ρ_2) is obtained introducing a matrix V_1 (V_2). To obtain the spectrum of \mathcal{F} we rewrite the expression for the diagonalized reduced density matrix ρ_2 in terms of the fermionic operators of the matrix ρ_1 which leads to $\rho_2 = e^{-H_2}$, where

$$H_2 = - \sum_{i=1}^L \sum_{j=1}^L \sum_{l=1}^L \left(\ln \frac{1 + \nu_{2,l}}{2} T_{l,i} T_{l,j} |1\rangle_i \langle 0|_i \otimes |0\rangle_j \langle 1|_j + \ln \frac{1 - \nu_{2,l}}{2} T_{l,i} T_{l,j} |0\rangle_i \langle 1|_i \otimes |1\rangle_j \langle 0|_j \right). \quad (16)$$

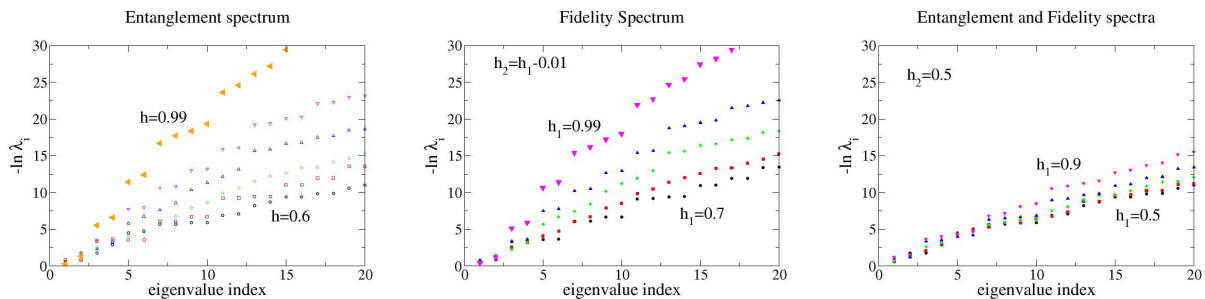


Figure 4: (color online) Fidelity spectrum $-\ln \lambda_i$, for system size $L = 6$. Left: entanglement spectrum for different values of magnetic field. From bottom to top $h = 0.6, 0.7, 0.8, 0.9, 0.95, 0.99$. Middle: fidelity spectrum for $\delta h = 0.01$ and for $h = 0.7, 0.8, 0.9, 0.95, 0.99$. Right: fidelity spectrum for pairs of the magnetic field as $h_1 = 0.5, h_2 = 0.5, 0.6, 0.7, 0.8, 0.9$.

Here

$$T_{l,i} = \sum_{p=1}^L \bar{V}_{2,l,p} (\bar{V})_{1,p,i}^{-1} \quad (17)$$

where we defined \bar{V} by

$$V = \bar{V} \otimes \begin{pmatrix} 0 & 1 \\ -1 & 0 \end{pmatrix}. \quad (18)$$

The diagonal elements $\nu_{2,l}$ are the diagonal elements of Ω for the magnetic field of ρ_2 . Diagonalizing H_2 , we obtain ρ_2 , expressed in the eigenbasis of ρ_1 , and obtain the spectrum of \mathcal{F} , as intended. Note that this requires diagonalizing a $2^L \times 2^L$ matrix which is much larger than the $L \times L$ matrix required for the entanglement entropy.

In Fig. 4 we show the fidelity spectrum $-\ln \lambda_i$. In the left panel we consider $\rho_1 = \rho_2$ and the operator \mathcal{F} is just the density matrix. Therefore, its logarithmic spectrum is the entanglement spectrum. In the middle panel we consider the fidelity spectrum and in the right panel we compare the entanglement spectrum with the fidelity spectrum. As discussed before [12] there is no clear structure in the entanglement spectrum since we are considering a real space block of spins. The fidelity spectrum when we consider two very close values of the magnetic field is very similar to the entanglement spectrum. In both cases as we increase the magnetic field and approach the critical point that separates the XX phase from the Ising phase, the entanglement or fidelity spectrum increases considerably. This implies that the fidelity operator spectrum is decreasing fast. The same can be seen when we compare the fidelity spectrum with the entanglement spectrum in the right panel. Here we are considering two values of the magnetic field h_1 and h_2 associated respectively with ρ_1 and ρ_2 that differ by a finite amount. Therefore there is a significant difference as the difference between h_1 and h_2 increases, even though we are far from the critical regime. The further the two points are the smaller the fidelity and the fidelity operator eigenvalues, λ_i , should be.

In order to analyse the spectrum we calculate the moments of the distribution of the eigenvalues [27] defined as

$$M_n = \sum_{i=1}^{2^L} \lambda_i^n. \quad (19)$$

The moment of order $n = 1$ is the fidelity. We also calculate the von Neumann entropy of the fidelity

$$S_1 = - \sum_{i=1}^{2^L} \lambda_i \ln \lambda_i \quad (20)$$

and the Rényi entropies

$$S_n = \frac{1}{1-n} \ln M_n. \quad (21)$$

Note that in the case of the entanglement ($\rho_1 = \rho_2$) the von Neumann entropy can also be obtained as

$$S_1 = - \sum_{i=1}^L \left(\frac{1+\nu_i}{2} \ln \frac{1+\nu_i}{2} + \frac{1-\nu_i}{2} \ln \frac{1-\nu_i}{2} \right) \quad (22)$$

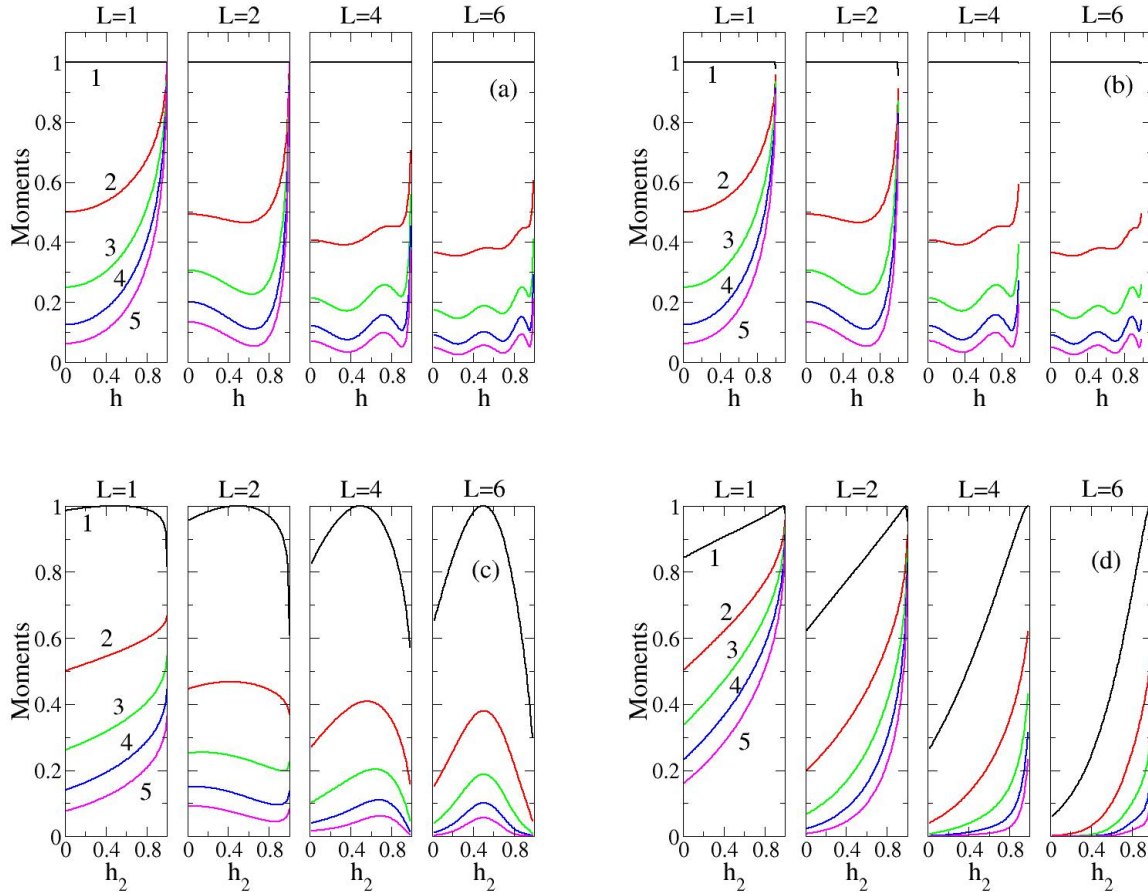


Figure 5: (color online) First five moments of the entanglement operator (density matrix) and fidelity operator spectra for blocks of sizes $L = 1, 2, 4, 6$, as a function of magnetic field. In the top left panel we consider the moments of the entanglement operator spectrum. In the top right panel we consider the moments of the fidelity operator spectrum for two close-by values of h . In the bottom left (right) panel we consider the fidelity operator spectra for $h_1 = 0.5$ ($h_1 = 0.98$) and h_2 arbitrary.

which only involves a sum with L terms.

In Fig. 5 we present the first five moments for several choices of pairs of magnetic fields (h_1, h_2) and for several block sizes, L . In the case of the entanglement spectrum, when $h_1 = h_2$, the first moment is just the trace of the density matrix (top left panel). When $h_1 \neq h_2$ it is the fidelity and therefore it is very close to 1 except in the vicinity of the phase transition where we consider $h_2 = h_1 - \delta h, \delta h = 0.01$ (top right panel). The higher momenta are very similar between the entanglement spectrum and the fidelity spectrum, in this case. A detailed study of the moments and Rényi entropies has been carried out in Ref. [28]. Considering two values of the magnetic fields further away from each other the moments change in structure. Fixing for instance $h_1 = 0.5$ (bottom left panel) or $h_1 = 0.98$ (bottom right panel) and varying h_2 we find that when h_2 crosses h_1 there is a sharp increase which equals one for the first moment (trivially since for this case the first moment is the trace of the density matrix). This maximum is also observed in the higher moments of the spectrum. A similar information can be obtained from the Rényi entropies. As explained above, S_1 is just the von Neumann entropy and the other entropies are proportional to the logarithms of the moments of the spectrum. In Fig. 6 we compare various cases for $L = 1, 6$. As the magnetic field approaches the critical point we find that the various entropies have a minimum near the critical point showing that the partial state density matrix signals the QPT, as previously obtained. In the lower panels we consider the Rényi entropies associated with the fidelity operator. The structure is in general more complicated. Fixing $h_1 = 0.98$ close to the critical point, as h_2 approaches h_1 the entropies tend to those corresponding to the entanglement spectrum. Far from this point the entropies differ considerably and depend strongly on the block size. For instance for $L = 1$ they are of the order of the entropies for the entanglement spectrum but for $L = 6$ the entropies are considerably higher, except the von Neumann entropy. Also, note that the Rényi entropy S_1 in the fidelity case has a depression at small magnetic fields.

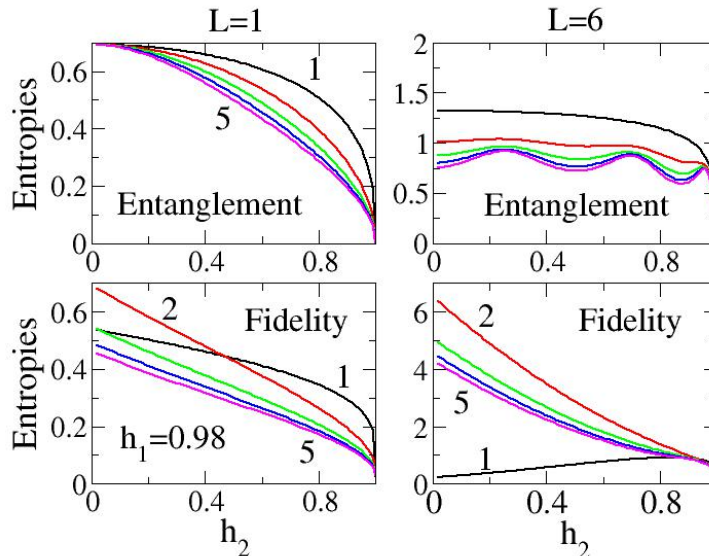


Figure 6: (color online) Rényi and von Neumann entropies for $L = 1$ (left) and $L = 6$ (right), for the first five moments, as a function of magnetic field. In the top panels we consider the entanglement operator spectrum and in the bottom panels the fidelity operator spectrum as a function of h_2 , for $h_1 = 0.98$. Note the decrease of the entropies close to the quantum critical point, both for the entanglement case and the fidelity case.

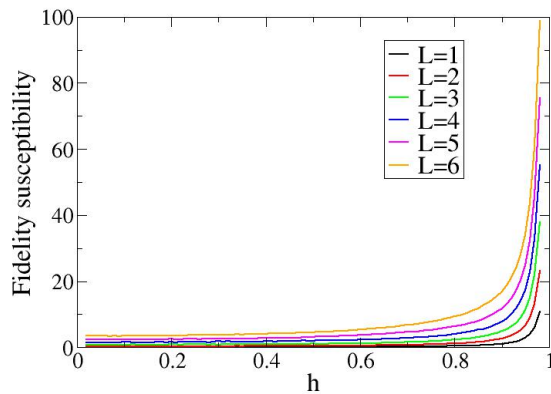


Figure 7: (color online) Block fidelity susceptibility as a function of magnetic field for $L = 1, \dots, 6$ which shows the sharp increase near the critical point.

We also calculate the fidelity susceptibility, introduced in [29] and [23], with its geometrical meaning discussed in [23, 30]. Global fidelity susceptibility for the XY model was discussed in [4, 23]. In the present paper we calculate the fidelity susceptibility associated to reduced density matrices of blocks of spins. It is defined as

$$\begin{aligned} \chi_F &= \sum_{i=1}^{2^L} \chi_{F,i} \\ \chi_{F,i} &= \frac{\partial^2 \lambda_i}{\partial(\delta h)^2}. \end{aligned} \quad (23)$$

In Fig. 7 we present the fidelity susceptibility associated with blocks of different sizes as a function of the magnetic field. The divergence of the susceptibility is clearly seen as we approach the QPT.

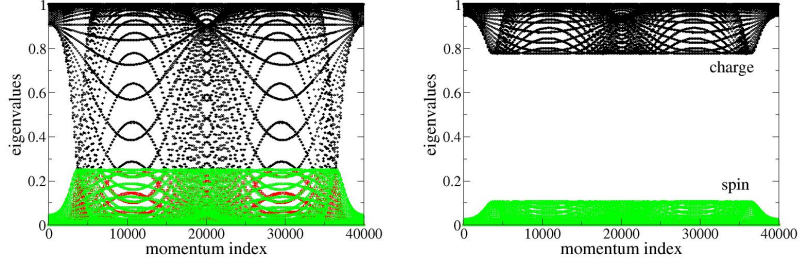


Figure 8: (color online) Exponential entanglement spectrum for a bulk superconductor as a function of momentum, labeled sequentially row by row in the Brillouin zone, in the normal phase ($\Delta = 0$, left panel), and in the superconducting phase ($\Delta \neq 0$, right panel), at temperature T . Note that in the right panel the lowest charge eigenvalue is smaller than the spin eigenvalues.

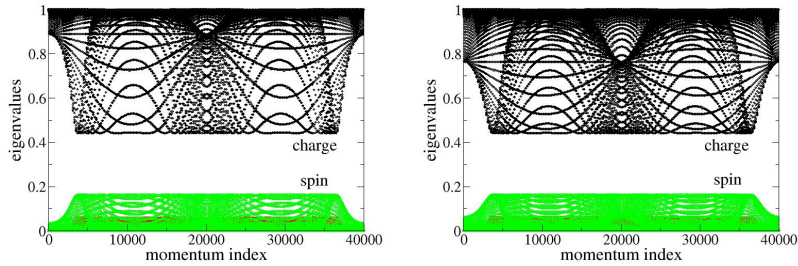


Figure 9: (color online) Fidelity operator spectrum for a bulk superconductor as a function of momenta, between the normal phase and the superconducting phase, at the same temperature (left) and at different temperatures (right).

IV. THERMAL STATES OF A CONVENTIONAL BCS SUPERCONDUCTOR

In this section we consider a conventional s -wave superconductor at finite temperature described by the effective mean-field BCS Hamiltonian

$$H_{BCS}^{eff} = \sum_k \varepsilon_k (n_{k\uparrow} + n_{k\downarrow}) - \sum_k (\Delta_k c_{k\uparrow}^\dagger c_{-k\downarrow}^\dagger + \Delta_k^* c_{-k\downarrow} c_{k\uparrow} - \Delta_k^* \langle c_{-k\downarrow} c_{k\uparrow} \rangle), \quad (24)$$

with $\Delta_k = -V \langle c_{-k\downarrow} c_{k\uparrow} \rangle$, where the lattice-mediated pairing interaction is constant and non-vanishing between electrons around the Fermi level only. The density matrix is given by [8]

$$\rho = \frac{1}{Z} e^{-(H_{BCS}^{eff} - \mu N)/T} = \frac{e^{\sum_k \vec{h}_k \vec{T}_k + K}}{\text{Tr}[e^{\sum_k \vec{h}_k \vec{T}_k + K}]} = \frac{\prod_k e^{\vec{h}_k \vec{T}_k}}{\prod_k \text{Tr}[e^{\vec{h}_k \vec{T}_k}]}, \quad (25)$$

where T is the temperature, $\vec{h}_k = (\tilde{h}_k^+, \tilde{h}_k^-, \tilde{h}_k^0) = (2\Delta_k^*/T, 2\Delta_k/T, -2\tilde{\varepsilon}_k/T)$, $\vec{T}_k = (T_k^+, T_k^-, T_k^0)$, $K = -1/T \sum_k (\tilde{\varepsilon}_k + \Delta_k^* b_k)$ and $\tilde{\varepsilon}_k = \varepsilon_k - \mu$. The norms of the vectors \vec{h}_k are given by $\tilde{h}_k = 2E_k/T$, with $E_k = \sqrt{\tilde{\varepsilon}_k^2 + |\Delta_k|^2}$. The coefficients $\vec{h}_k = \vec{h}_k(T, V)$ are functions of both the coupling constant V and the temperature T , through the gap parameters $\Delta_k = \Delta_k(T, V)$ and the chemical potential μ . By $n_{k\sigma} = c_{k\sigma}^\dagger c_{k\sigma}$ we denote the one-particle number operators, while by $b_k^\dagger = c_{k\uparrow}^\dagger c_{-k\downarrow}^\dagger$ and $b_k = c_{-k\downarrow} c_{k\uparrow}$. The T_k operators are given by $T_k^+ = b_k^\dagger$, $T_k^- = b_k$ and $2T_k^0 + 1 = (n_{k\uparrow} + n_{-k\downarrow})$ and form a $\text{su}(2)$ algebra.

The fidelity is given by

$$F(\rho_a, \rho_b) = \text{Tr}[(\rho_a^{1/2} \rho_b \rho_a^{1/2})^{1/2}] = \frac{\text{Tr}[(\prod_k e^{\frac{\tilde{a}_k}{2} \vec{T}_k} e^{\vec{b}_k \vec{T}_k} e^{\frac{\tilde{a}_k}{2} \vec{T}_k})^{1/2}]}{\prod_k (\text{Tr}[e^{\tilde{a}_k \vec{T}_k}] \text{Tr}[e^{\vec{b}_k \vec{T}_k}])^{1/2}} = \text{Tr} \left[\prod_k (\mathcal{F}_k)^{1/2} \right]. \quad (26)$$

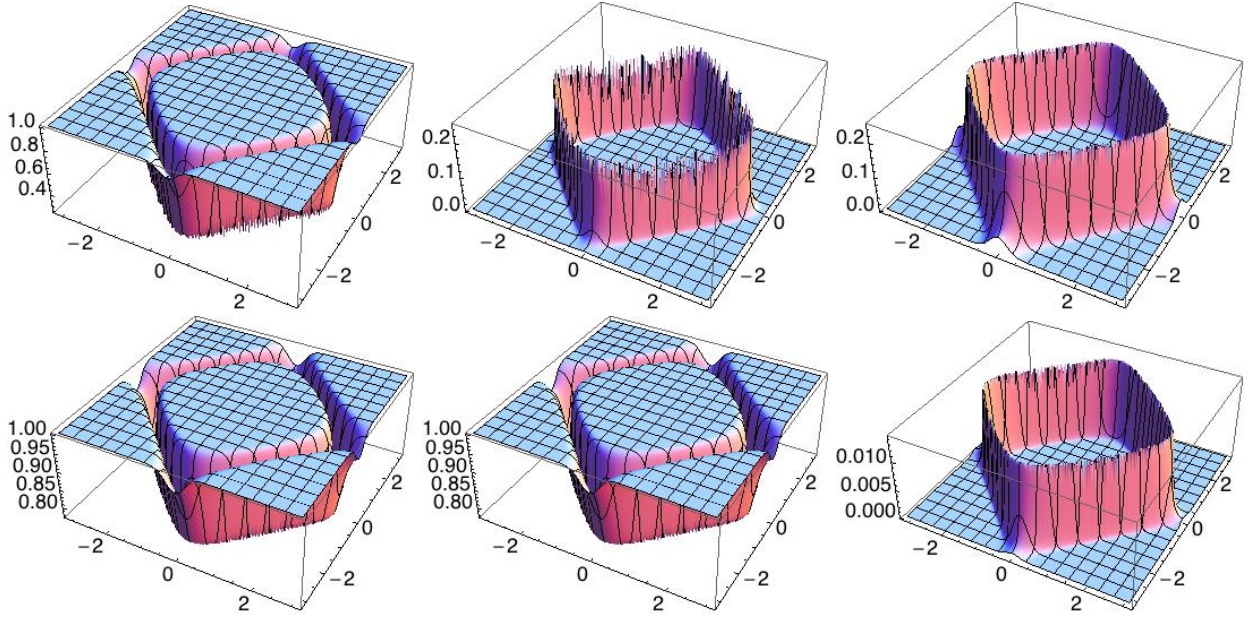


Figure 10: (color online) Top (bottom) panels: normal (superconducting) phase exponential entanglement spectrum. In the three panels we show three eigenvalues since the two spin eigenvalues are degenerate.

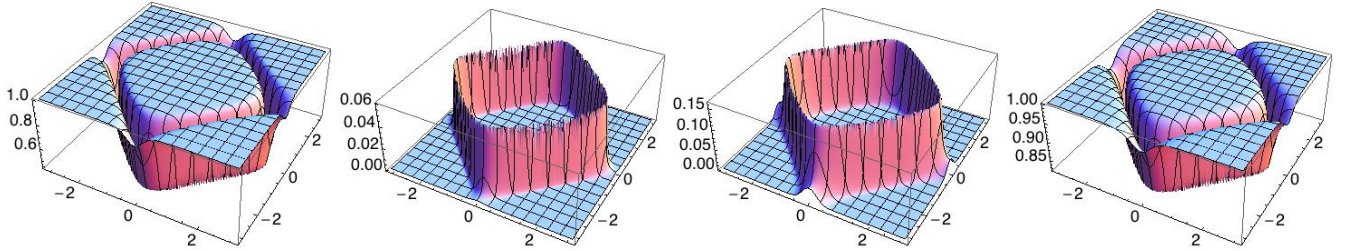


Figure 11: (color online) Fidelity operator spectrum between superconducting and normal phases. In the first 3 panels we show the 3 eigenvalues and in the last one the fidelity (smaller than 1 close to the Fermi surface). Note that the temperature is the same, with Δ either finite (superconducting phase) or zero (normal phase).

As for every k the operators \bar{T}_k form a $\text{su}(2)$ algebra, and therefore by exponentiation define a Lie group, we can write $e^{\frac{\bar{a}_k}{2}\bar{T}_k}e^{\bar{b}_k\bar{T}_k}e^{\frac{\bar{a}_k}{2}\bar{T}_k} = e^{2\bar{c}_k\bar{T}_k}$. For each value of the momentum we get a 4-dimensional space respecting to momentum states that are empty, doubly occupied or singly occupied by a spin up or a spin down electron. The space is therefore of the type $\mathcal{B} = \{|0\rangle, |\uparrow\downarrow\rangle, |\uparrow\rangle, |\downarrow\rangle\}$, similarly to the problem of the impurity in a superconductor. The fidelity operator is then easily diagonalized in this 4×4 subspace. We will study the possible eigenvalues of the fidelity operator for each momentum. As before, the charge and spin parts separate. Moreover, in this problem the two spin components are degenerate. Therefore it is enough to look at three eigenvalues (two for the charge part and one for the spin part). The results are presented in the Figs. 8-12 and discussed in more detail below.

The fidelity operator for each momentum value (denoted k -fidelity operator) is of the form $\mathcal{F}_k = \sqrt{A_k}$, where

$$A_k = \frac{1}{D_k} \begin{pmatrix} \alpha_k & \beta_k & 0 & 0 \\ \beta_k & \gamma_k & 0 & 0 \\ 0 & 0 & 1 & 0 \\ 0 & 0 & 0 & 1 \end{pmatrix}. \quad (27)$$

The matrix elements are given by

$$\begin{aligned}\alpha_k &= \cosh E_k^a/T \cosh E_k^b/T + \sinh E_k^a/T \sinh E_k^b/T \frac{\Delta_k^a \Delta_k^b + \bar{\epsilon}_k^a \bar{\epsilon}_k^b}{E_k^a E_k^b} \\ &+ \sinh E_k^a/T \cosh E_k^b/T \frac{\bar{\epsilon}_k^a}{E_k^a} + \sinh E_k^b/T \frac{\bar{\epsilon}_k^b}{E_k^b} \\ &+ (\cosh E_k^a/T - 1) \sinh E_k^b/T \frac{\Delta_k^a \Delta_k^b + \bar{\epsilon}_k^a \bar{\epsilon}_k^b}{E_k^a E_k^b} \frac{\bar{\epsilon}_k^a}{E_k^a}\end{aligned}\quad (28)$$

$$\begin{aligned}\gamma_k &= \cosh E_k^a/T \cosh E_k^b/T + \sinh E_k^a/T \sinh E_k^b/T \frac{\Delta_k^a \Delta_k^b + \bar{\epsilon}_k^a \bar{\epsilon}_k^b}{E_k^a E_k^b} \\ &- \sinh E_k^a/T \cosh E_k^b/T \frac{\bar{\epsilon}_k^a}{E_k^a} - \sinh E_k^b/T \frac{\bar{\epsilon}_k^b}{E_k^b} \\ &- (\cosh E_k^a/T - 1) \sinh E_k^b/T \frac{\Delta_k^a \Delta_k^b + \bar{\epsilon}_k^a \bar{\epsilon}_k^b}{E_k^a E_k^b} \frac{\bar{\epsilon}_k^a}{E_k^a}\end{aligned}\quad (29)$$

$$\begin{aligned}\beta_k &= \sinh E_k^a/T \cosh E_k^b/T \frac{\Delta_k^a}{E_k^a} + \sinh E_k^b/T \frac{\Delta_k^b}{E_k^b} \\ &+ (\cosh E_k^a/T - 1) \sinh E_k^b/T \frac{\Delta_k^a \Delta_k^b + \bar{\epsilon}_k^a \bar{\epsilon}_k^b}{E_k^a E_k^b} \frac{\Delta_k^a}{E_k^a}\end{aligned}\quad (30)$$

and

$$D_k = 2(1 + \cosh E_k^a/T) 2(1 + \cosh E_k^b/T). \quad (31)$$

The eigenvalues of the k -fidelity operator, \mathcal{F}_k are therefore of the form

$$\frac{1}{\sqrt{D_k}} \begin{pmatrix} \eta_+^k & 0 & 0 & 0 \\ 0 & \eta_-^k & 0 & 0 \\ 0 & 0 & 1 & 0 \\ 0 & 0 & 0 & 1 \end{pmatrix}, \quad (32)$$

where

$$\eta_{\pm}^k = \frac{1}{2} \left[(\alpha_k + \gamma_k) \pm \sqrt{(\alpha_k - \gamma_k)^2 + 4\beta_k^2} \right]. \quad (33)$$

We will be interested in situations where ρ_1 and ρ_2 correspond to points in parameter space, which we choose to be the temperature, T , and the gap function, Δ_k , that are far apart and may be in the same or different thermodynamic phases.

In Fig. 8 we present the k -fidelity operator spectrum (of the operator \mathcal{F}_k) for the case when the two density matrices are equal (“exponential entanglement spectrum”) where we compare the system in the normal phase (left) with the superconducting phase (right). The horizontal axis is an index over the eigenvalues and in the vertical axis we plot λ_k . We only plot three eigenvalues because the spin eigenvalues are degenerate. For each label the sum over the four eigenvalues is 1 due to normalization. In both phases the higher eigenvalue is the charge eigenvalue corresponding to empty sites (this will be discussed later on). In the normal phase the lowest eigenvalues merge into the higher eigenvalues but in the superconducting phase the energy gap is clearly visible. Note that the eigenvalues are now labeled by the momentum. There is no partitioning of the system in real space but there is a partitioning of the system in momentum space (since the system can be block diagonalized). Recall however that here the mixed state originates in the thermal states. We stress that we are not plotting the fidelity operator, $\mathcal{F} = \prod_k \mathcal{F}_k$, eigenvalues. In Fig. 9 we consider two different density matrices where we plot the k -fidelity operator spectrum where one of the density matrices corresponds to a point in phase space in the normal phase and the other in the superconducting phase. In the left panel the temperatures, T_a, T_b , are the same (this can be obtained for instance considering two coupling constants) and in the right panel the temperatures, T_a, T_b , are different. In the first case the gap is still clearly visible. When the temperatures are different the gap remains the same. There is a small decrease of the highest charge eigenvalue that can be traced to the vicinity of the Fermi surface, as shown ahead.

In order to understand the spectrum in greater detail we consider the various eigenvalues in momentum space. In Fig. 10 we consider the system in the normal phase and in the superconducting phase for two equal density

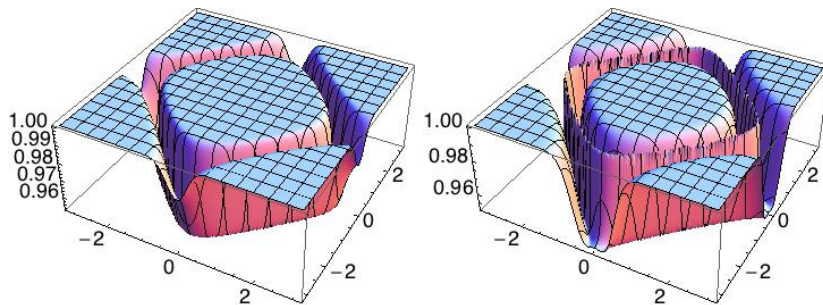


Figure 12: (color online) Total fidelity as a function of momentum. Left panel: different temperatures and same finite Δ ; right panel: different temperatures and $\Delta = 0$.

matrices $\rho_a = \rho_b$ and plot the three eigenvalues of the k -fidelity operator as a function of momentum, for a 2d system. The fidelity is one for all momenta since $\text{Tr}\rho_a = \text{Tr}\rho_b = 1$. The depression in the highest eigenvalue (left panels) marks clearly the Fermi surface. For momenta larger than the Fermi momentum there are no electrons (except for thermal excitations contained in the Fermi function). So the eigenvalue corresponding to empty states is 1. The other eigenvalues are close to zero outside the Fermi surface. Due to the particle-hole transformation of the Bogoliubov transformation, the empty site eigenvalue (corresponding to doubly occupied sites in terms of the electrons) is also close to 1 inside the Fermi surface. Accordingly, the other eigenvalues are also close to zero inside the Fermi surface. The noticeable features are therefore close to the Fermi surface. A similar structure is observed in the superconducting phase. There is a slight change close to the Fermi surface which is due to the opening of the superconducting gap. The amplitude of the doubly occupied and spin eigenvalues are smaller in this case since the decrease of the first eigenvalue is smaller along the Fermi surface.

In Fig. 11 we show the fidelity operator spectrum for the case when one density matrix is in the normal phase and the other corresponds to a quantum state in the superconducting phase. The last panel shows the total fidelity. It is significantly decreased around the Fermi surface where the difference between the normal phase and the superconducting phase is larger due to the pairing and opening of the gap. Note that the highest eigenvalue has a structure that strongly resembles the total fidelity.

Finally, in Fig. 12 we compare the total fidelity as a function of momentum for different temperatures. The right panel corresponds to two quantum states in the normal phase but at different temperatures. As expected, around the Fermi surface the fidelity decreases however there is a sharp region where it approaches one. The width of the region around the Fermi surface is determined by the temperature through the Fermi function. The sharp maximum corresponds to the point where the two Fermi functions cross and so it pinpoints the location of the Fermi surface.

V. CONCLUSIONS

We have introduced and analysed the fidelity spectrum and the fidelity operator spectrum for partial states for different systems such as a magnetic impurity in a conventional superconductor, a XX spin-1/2 chain in a transverse magnetic field and the thermal states of a finite temperature bulk superconductor.

In the first problem we have found that only one charge eigenvalue and one spin eigenvalue have important changes as the quantum phase transition induced by the magnetic impurity occurs. The transition is associated with the capture of one electron by the impurity with a parallel spin. This feature is clearly seen when we consider two density matrices associated with the same lattice site (particularly the impurity site) and different but close by spin couplings between the impurity and the spin density of the electrons. Selecting two density matrices with the same spin coupling but different lattice sites leads to a signature of the phase transition that can be seen both from the eigenvalues associated with lattice sites far from each other and from the same lattice site.

In the spin chain problem we have studied for the first time the block fidelity and the block fidelity susceptibility and found that the quantum phase transition that occurs between a XX phase and an Ising like phase is well signaled by the block fidelity. Both the entanglement spectrum and the fidelity spectrum do not show any significant features and we analysed the spectra calculating the moments of the distribution and the Rényi entropies. The S_1 Rényi entropy associated with the block fidelity shows a distinctive characteristic away from the critical point.

Finally, in the finite temperature bulk superconductor we showed that in the superconductor there is a clear gap between the various k -eigenvalues, as for the energy spectrum. In the case of two different density matrices we found that the effect of temperature is stronger than the difference in the order parameter distinguishing the normal from

the superconducting phase. Analysing the k -fidelity operator spectrum it was clearly seen that the properties are determined by the structure around the Fermi energy, as expected. In the case of two density matrices for different temperatures in the normal phase the fidelity has a sharp maximum at the location of the Fermi surface, determined by the crossing of the Fermi functions.

We have shown that the fidelity spectrum, which we have introduced, can give a more detailed description and characterization of the phase transitions of many-body quantum systems providing complementary information to other techniques. Therefore, we hope that this can be applied to non-trivial problems where the traditional Ginzburg-Landau theory with a local order parameter is not known.

Acknowledgments

NP thanks the project of SQIG at IT, funded by FCT and EU FEDER projects QSec PTDC/EIA/67661/2006 and QuantPrivTel PTDC/EEA-TEL/103402/2008, IT Project QuantTel, and Network of Excellence, Euro-NF. VRV and PDS thank the project PTDC/FIS/64926/2006, of Fundação para a Ciência e a Tecnologia, Portugal.

-
- [1] W. K. Wootters, Phys. Rev. D **23**, 357 (1981).
 - [2] H. Li and F.D.M. Haldane, Phys. Rev. Lett. **101**, 010504 (2008).
 - [3] L. Amico, R. Fazio, A. Osterloh, and V. Vedral, Rev. Mod. Phys. **80**, 517 (2008).
 - [4] P. Zanardi and N. Paunković, Phys. Rev. E **74**, 031123 (2006).
 - [5] S.J. Gu, Int. J. Mod. Phys. B **24**, 4371 (2010).
 - [6] H.Q. Zhou, arXiv:0704.2945.
 - [7] N. Paunković, P.D. Sacramento, P. Nogueira, V.R. Vieira and V.K. Dugaev, Phys. Rev. A **77**, 052302 (2008).
 - [8] N. Paunković and V.R. Vieira, Phys. Rev. E **77**, 011129 (2008).
 - [9] N. Regnault, B. A. Bernevig, and F. D. M. Haldane, Phys. Rev. Lett. **103**, 016801 (2009).
 - [10] D. Poilblanc, Phys. Rev. Lett. **105**, 077202 (2010).
 - [11] A. Sterdyniak, N. Regnault, and B. A. Bernevig, Phys. Rev. Lett. **106**, 100405 (2011).
 - [12] R. Thomale, D.P. Arovas and B.A. Bernevig, Phys. Rev. Lett. **105**, 116805 (2010).
 - [13] A. Sakurai, Prog. Theor. Phys. **44**, 1472 (1970).
 - [14] A.V. Balatsky, I. Vekhter and J.-X. Zhu, Rev. Mod. Phys. **78**, 373 (2006).
 - [15] P.D. Sacramento, P. Nogueira, V.R. Vieira and V.K. Dugaev, Phys. Rev. B **76**, 184517 (2007).
 - [16] E. Lieb, T. Schultz and D. Mattis, Annals of Phys. **16**, 407 (1961).
 - [17] E. Barouch and B. McCoy, Phys. Rev. A **3**, 786 (1971).
 - [18] G. Vidal, J.I. Latorre, E. Rico and A. Kitaev, Phys. Rev. Lett. **90**, 227902 (2003).
 - [19] J.I. Latorre, E. Rico and G. Vidal, Quant. Inf. Comput. **4**, 48 (2004).
 - [20] B.-Q. Jin and V.E. Korepin, J. Stat. Phys. **116**, 79 (2004).
 - [21] P. Zanardi, M. Cozzini, and P. Giorda, J. Stat. Mech. **2**, L02002 (2007).
 - [22] M. Cozzini, P. Giorda, and P. Zanardi, Phys. Rev. B **75**, 014439 (2007).
 - [23] P. Zanardi, P. Giorda, and M. Cozzini, Phys. Rev. Lett. **99**, 100603 (2007).
 - [24] D. F. Abasto, N. T. Jacobson, and P. Zanardi, Phys. Rev. A **77**, 022327 (2008).
 - [25] S. Garnerone, N. T. Jacobson, S. Haas and P. Zanardi, Phys. Rev. Lett. **102**, 057205 (2009).
 - [26] J. Dubail and J.-M. Stéphan, J. Stat. Mech. **3** L03002 (2011).
 - [27] F. Pollmann and J.E. Moore, New J. Phys. **12**, 025006 (2010).
 - [28] A. R. Its and V. E. Korepin, J. Stat. Phys. **137**, 1014 (2009).
 - [29] W. L. You, Y. W. Li and S. J. Gu, Phys. Rev. E **76**, 022101 (2007).
 - [30] L. Campos Venuti and P. Zanardi, Phys. Rev. Lett. **99**, 095701 (2007).